# Fully Automatic Abdominal Fat Segmentation System from a Low Resolution CT Image

Pan-Fu Kao[1,2]       Yu-Liang Kuo[3,4]       Po-Tsun Lai[5]       Wei-Chen Chen[5]

Ya-Ling Hsu[5]       Chiun-Li Chin[5,*]

[1] Director, Dept. of Nuclear Medicine, Chung Shan Medical University Hospital

Taichung 402, Taiwan, ROC

[2] School of Medicine, Chung Shan Medical University

Taichung 402, Taiwan, ROC

pfkao@csmu.edu.tw

[3] School of Medical Imaging and Radiological Sciences, Chung Shan Medical University

Taichung 402, Taiwan, ROC

[4] Dept. of Medical Imaging, Chung Shan Medical University Hospital

Taichung 402, Taiwan, ROC

yuliangkuo@csmu.edu.tw

[5] School of Medical Informatics, Chung Shan Medical University

Taichung 402, Taiwan, ROC

ernestli@csmu.edu.tw

**Abstract.** As the prevalence of obesity continues to rise with lifestyle changes in recent years, accurate tools for quantifying abdominal body and organ fat are critically needed to assist researchers investigating therapeutic and preventive measures against obesity and its comorbidities. Fatty infiltration of the liver, pancreas, and skeletal muscles are indicators of diabetes, the metabolic syndrome, and obesity. In this paper, it is important to be able to calculate the amount of abdominal fat for diagnosing cardiovascular disease or metabolism disease. Therefore, we propose a fully automatic abdominal fat segmentation system for quantifying abdominal fat, including subcutaneous adipose tissue and visceral adipose tissue. It can be divided into three parts. First, the abdominal region is assessed from a low resolution CT image. Next, the boundary line between subcutaneous adipose tissue (SAT) and visceral adipose tissue (VAT) is found using our proposed methods. Finally, the amount of abdominal fat in the SAT or VAT regions is calculated. From experiment results, our proposed system has a higher than 90% successful rate for distinguishing the SAT and VAT regions based on a level consistency error and a detection rate index. And, it has average 82% successful rate from calculating artificial assessment evaluated by the two radiologists.

**Keywords:** subcutaneous adipose tissue, visceral adipose tissue, total adipose tissue, CT images, segmentation of abdominal fat.

## 1 Introduction

The abdomen of the human body is the part located between the pelvis and chest. In terms of function, the abdomen is the location of most parts of the digestive tract, implying that digestion and absorption occur in the abdomen. The esophagus, stomach, duodenum, rectum, appendix, and so on are all in the abdomen, along with the liver, kidney, pancreas, spleen and other essential organs. Abdominal adipose tissues can be divided into two categories, subcutaneous adipose tissue (SAT) and visceral adipose tissue (VAT).

   SAT, a layer of rather loose tissue, is a natural buffer to cushion the outside pressure, and it is also an insulator to retain heat which is helps to restore energy. Besides adipose tissue, there are also blood vessels, lymphatic channels, nerves, sweat glands, and hair follicles. VAT is located around the abdominal organs such as stomach

---

* Corresponding author: Chiun-Li Chin, e-mail: ernestli@csmu.edu.tw, School of Medical Informatics, Chung Shan Medical University, No.110, Sec.1, Jianguo N.Rd., Taichung City 40201,Taiwan. Tel: 886-4-24730022 ext. 12186

and intestines. The function of the fat tissues, in addition to a source of metabolic energy, is to protect organs from injury caused by collision and to preserve the proper location of organs.

However, according to many studies, excessive adiposity is related to the occurrence of hypertension, diabetes, hyperlipidemia, and cardiovascular disease [1]. Living in the era of industrialization, commercialization, and technological advancement, modern people tend to sit for a long time, having high caloric diets, abnormal life style, and a lack of exercise [2]. These have led to a rapid increase in overweight and obese children, adults, and elderly people [3-5]. Among these groups, a long-term research goal for 2 to 19 year-old children has been to determine body mass indices (BMI) for age growth charts [6]. Also for adults above 20 and elderly people, a goal of research has been to determine the rates of various comorbidities associated with overweight and obesity by sex, age, and group [7].

Therefore, to better understand the relationships between overweight and obesity in modern society as they relate to health, we aimed to study thoroughly the interior and exterior fat in the abdomen, making it easier for the research personnel to comprehend how obesity affects people's health in daily life [8].

Researchers in the area of medical image analysis have long sought to extract contours of different body organs and tissue types from medical images of various modalities. The objective evaluation of these medical image segmentation methods on a large clinical dataset is one of the important steps toward establishing validity and clinical applicability of an algorithm.

In previous research of the segmentation of abdominal fat tissue, we discovered that there are many manual and automatic methods to determine the image of abdominal fat. We also found that most of the research relies on MRI images rather than CT images. Generally, the amount and time of CT scan are less than MRI. And, CT image has a higher image quality than MRI. Hence, people are more general to use CT scan than MRI. In view of this, we use the CT images as the object of our research. In this paper, we evaluated the use of low resolution CT images to quantify abdominal fat deposits. Before new techniques for the segmentation of abdominal fat tissue were invented, physicians needed to use their eyes and hands to depict the adipose deposits in the abdomen on a computerized abdominal image via medical software. The manual job takes time. Using CT images for example, the semi-automatic system described by X.J. Li et al. [9] revealed total adipose tissue (TAT) sections by segmenting via computer software. When circling the VAT section, they distinguished the adipose tissues from non-adipose tissues by segmentation of tissue manually. This was very labor intensive.

A. Pednekar et al. [10] proposed the segmentation of abdominal fat tissue from CT images. This method combines the intensity and texture information with local "hanging togetherness" within a tissue class. The results definitely display the segmented adipose image. However, they did not distinguish between the SAT and VAT. H. Chung et al [11] reported an automated method for segmentation of individual structures in the soft tissue with CT images. Adipose tissue was separated from the musculature but individual structures were not identifiable. Y. Jin et al. [12] presented a hybrid segmentation method that provided robust delineation results for adipose tissue from whole body MRI scans. H. Bertram et al. [13] segmented the abdominal images via software as well as manual procedures. A. Zhou et al. [14] also presented a fully-automated abdominal fat quantification method for rapid and accurate SAT and VAT measurement. According to our observations, most of the earlier studies emphasized MRI images; only a few of them used CT images as the basis for the research.

Therefore, focusing on the efficiency of the manual and automatic segmentation, and the problem of minor detection on CT images, we developed an automatic system of segmentation of abdominal fat tissue from CT images using medical knowledge from physicians to ensure the location of adipose tissues. During the process, we used pattern recognition technologies to develop segmentation results comparable to the results of manual procedures but with greater efficiency than procedures for manual and semi-automatic segmentation. It not only has high accuracy and high credibility with the manual methods but will also allow investigators to do research more conveniently and quickly. They can understand the content of the adipose from both inside and outside the abdomen which would improve the possibility of better understanding pathological changes individuals.   This would help physicians to develop better strategies for treatment and prevention [15-17].

Quantifying the performance of a segmentation algorithm is a very important task. In general, evaluation method for image segmentation can be classified into analytical and empirical evaluation methods [18]. The analytical methods of evaluation typically focus on analyzing the properties of a segmentation algorithm, such as its processing strategy, complexity, and efficiency. In this paper, we use objective level consistency error measure [19] to evaluate the results of our segmentation. It is an empirical evaluation method. Overall cross entropy (OCE) is a new empirical discrepancy error measure which quantifies the similarity or discrepancy between a segmented image and the ground truth image at the object level. The error measure takes into account the existence, size, position, and shape of each fragment and penalizes both over-segmentation and under-segmentation. This will improve the errors of the image division through the objective evaluation of OCE and thus increase the usability of the automatic system.

The objective of this study was to combine the advantages of the radiologist's knowledge and pattern recognition techniques to develop an automatic segmentation system for distinguishing SAT and VAT and the amount of abdominal fat seen on low resolution abdominal CT images. The major features of the proposed system are 1) the abdominal region is imaged, 2) a boundary line-seeking and link algorithm are proposed, and 3) the amount of abdominal fat is calculated.

Subsequently, the rest of the paper is organized as follows. In the section 2, we divide the procedure into abdominal region extraction, boundary line-seeking between SAT and VAT, and calculation of the amount of abdominal fat. We put emphasis on the process of imaging the inner and outside parts. The methods we developed include the extraction of the TAT edge, segmentation processing, denoising, and searching for boundaries between the SAT and VAT, and usage of the abdominal images. The experimental results in Section 3 demonstrate the images of VAT and SAT after performing our proposed method for segmentation and evaluate the result of our segmentation. In the section 4, the discussion of experimental result is presented. Finally, in section 5, we provide a conclusion, analysis and comparison of the results.

## 2 Materials and Methods

In this paper, we propose an automatic segmentation system for quantifying abdominal fat. The whole processing procedure of this system is shown in Fig. 1. The system is divided into three parts. First, it is the abdominal region imaging. The system will read an abdominal CT image, improve the brightness and contrast of the image, and cut out the abdominal area. Second, for finding the boundary line between SAT and VAT, we have to first identify the TAT area and divide the abdominal area into smaller areas, remove the organs not belonging to adipose tissue as well as other tissues, and then clear out the noises of the isolated adipose image. After the procedures above are finished, the TAT image will be created using the known TAT image to search for the boundary line between SAT and VAT using our boundary line-seeking method. Third, we will use the proposed linking algorithm to complement the leak between lines to obtain a complete boundary line. Finally, we can calculate the fat quantity of SAT and VAT, respectively. In the following we will explain every procedure in detail.
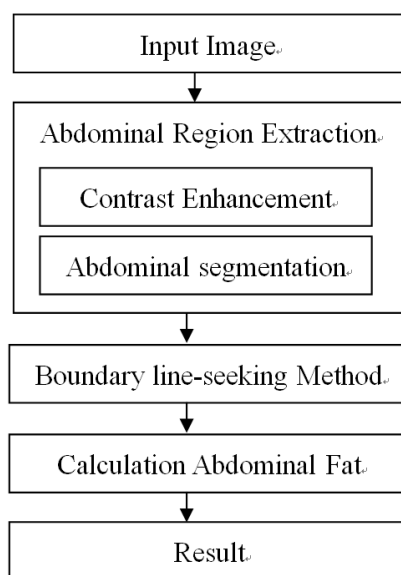


**Fig. 1.** The flowchart of abdominal fat detection.

### 2.1 Abdominal Region Demarcation

#### A.   Contrast enhancement

In the pre-processing, after entering a low-resolution original abdominal CT image, as shown on Fig. 2(a), we can see from the figure that the image contrast is not sufficient, so we enhance the contrast of the abdominal CT image to make the whole adipose tissue, the non-adipose tissues and the organs all displayed more clear by increasing the contrast between the various tissues. Here we use the cubic curve contrast enhancement method [20-21] to make the image contrast more obvious and its texture clearer. This method was proposed by Lin in 2006 [22]. Fig. 2(b) shows the cubic function of contrast enhancement curve. According to the different contrast degree in original image, we can control the position of inflection point to increase the luminance of darkness part and reduce the luminance of brightness part in the image. From the content of original image, we find out the coordinate (*A, B*) of the inflection point and then enhance the image contrast.
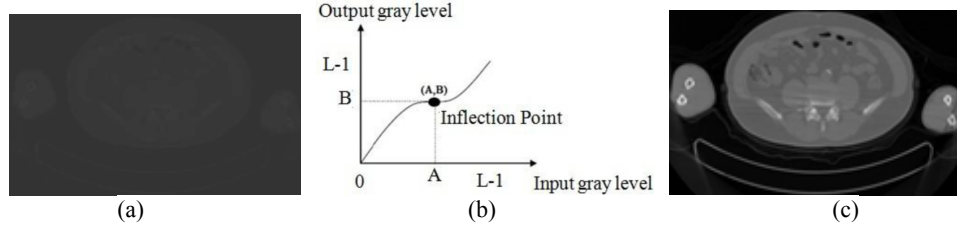
**Fig. 2.** (a) The original abdominal image, (b) The cubic curve of contrast enhancement method, and (c) The result image obtained after performing contrast enhancement.

Equation (1) shows the cubic curve equation; here x represents the pixel value of the original image, and y represents that of the intensified image. Because the curve passes through the origin (0, 0); d can be omitted.

$$y = f(x) = ax^3 + bx^2 + cx + d \tag{1}$$

Before the correlated coefficients a, b and c are calculated, Eq. (2) is used to find the x coordinate A of the inflection point. When we determined what the inflection point was, the contrast-enhanced cubic curve was obtained immediately. Hence, a proper inflection point can determine any point along the contrast-enhanced curve and adjust for the effect of enhanced image contrast.

$$A = \min_{x \in I}\{x\} + 0.7(\max_{x \in I}\{x\} - \min_{x \in I}\{x\}) \tag{2}$$

In Eq. (2), A represents the x coordinate of the inflection point, I represents an image, and x is any one of the pixel values in the image. Then, based on equations (3), (4) and (5), we can calculate the contrast-enhanced cubic curve.

$$c = 1 - a \times (255)^2 - b \times 255 \tag{3}$$

$$b^3 = 3 \times a - (255)^2 \times 3a^2 - 255 \times 3 \times a \times b \tag{4}$$

$$a = \frac{1}{(255)^2 - 3 \times 255 \times A + 3 \times A^2} \tag{5}$$

We discovered that the contrast-enhanced curve was related with inflection point in equation (5). The following procedure, from steps 1 to 5, was used obtained the contrast-enhanced curve, shown as the follows:

Step 1: Arbitrarily chosen value of A, whose range was between 0 and 255.
Step 2: A was given a value in equation (2) for solving the value of a.
Step 3: When the value a and A were known, the value of b can be obtained by equation (4).
Step 4: When the value of the a and b variables were known, the value of c was determined by by equation (3).
Step 5: When the values a, b and c were determined, the contrast-enhanced cubic curve was obtained.

Finally, Fig. 2 (c) shows the result after performing the image contrast enhancement. From the figure we can obviously see that in the abdominal CT image every tissue and region is clearly shown.

### B. Abdominal segmentation

Then we have to obtain the preliminary abdominal image from Fig. 2 (c), but the biggest problem is that there is not only the abdominal area in the CT image we had obtained; there the disruption of the hand and the long strip at the bottom is included. Based on this reason, we use an Otsu algorithm [23] to obtain a binarized threshold value and binarize the contrast-enhanced Fig. 2 (c) to make the disruptors and the abdominal area clearly distinguishable. The result is as shown on Fig. 3 (a).

From the binarized abdominal image in Fig. 3(a), we know that the large white area in the middle is the abdominal area. Because there is the disruption of the long strip, we will use an image projection method to remove the unneeded blocks. It allows us to clearly cut out the abdominal area. Fig. 3 (b) shows that there are two diagrams to explain the vertical and horizontal of image projection. And, the image projection equation is as displayed below:

The horizontal projection of binarized image: $\quad P(y) = \sum_{x=1}^{width} I(x, y) \tag{6}$

The vertical projection of binarized image:

$$P(x) = \sum_{y=1}^{height} I(x, y)$$
(7)

where $I(x, y)$ is the binarized image which needs projection, and width and height are the width and height of the projection-needing image; $P(x)$ and $P(y)$ indicates the histogram of vertical and horizontal projection of the binarized image, respectively.
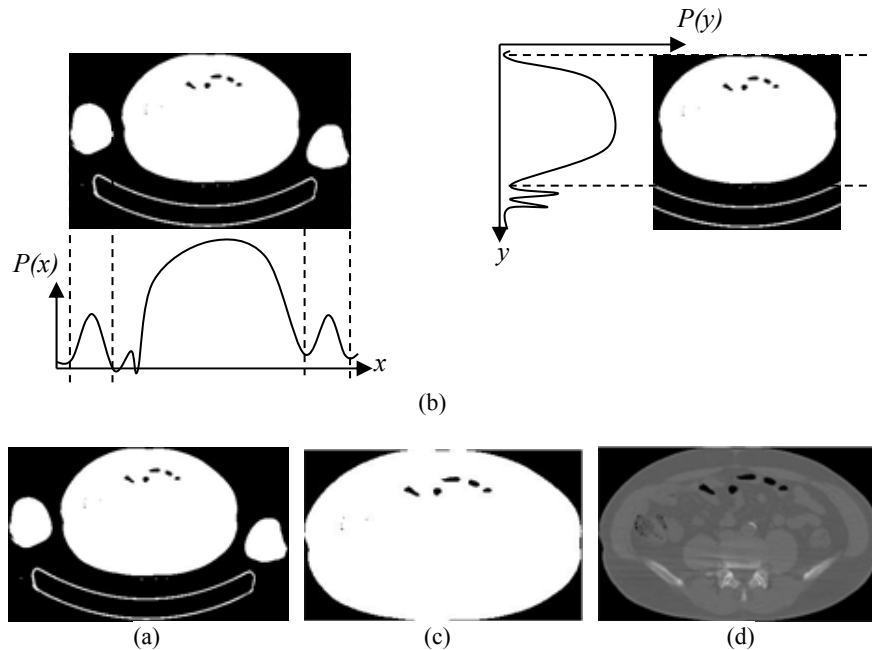


(b)



(a)                              (c)                              (d)

**Fig. 3.** (a) The binarized abdominal image, (b) There are two diagrams to explain the vertical and horizontal of image projection, (c) Abdominal binarized image after performing image projection, and (d) The abdominal image in the original image.

After performing image projection, we will obtain the binarized abdominal image as shown in Fig. 3(c). Next, we need to recognize the tissue inside the abdominal space. Finally we use the binarized abdominal image to revert its original image information as shown in Fig. 5. The result is as shown in Fig. 3(d).

## 2.2 Boundary line-seeking Method

For distinguishing the SAT and VAT, we proposed a boundary line-seeking method to achieve this task. Herein, it is divided into two parts: TAT area extraction and SAV/VAT area extraction. The following sections will be described in detailed.

### A. TAT Area Extraction

After performing abdominal region preparations, we obtained the initial abdominal CT images. For the purpose of measuring the fat area, we used the Otsu algorithm to obtain the binarization threshold value from the image by fat and non-fat regions, and performed image binarization on the abdomen image as shown in Fig. 3(c). The non-fat region is the white color in the image as shown in Fig. 4(a). Next, we performed the XOR operator between the binarized abdomen image and non –fat area image to get an abdominal fat area image. The white regions in the image represent fat area as shown in Fig. 4(b).

After obtaining the pure fat area of the image, we found that the outer edge was not smooth. Because the image we used is a low-resolution CT images we extracted a lot of small noises in the image.   The distribution range of the noise was so broad that the noise covered the fat area. The above problem will increase detection error in the results, and it is difficult to find the boundary line between the SAT and VAT areas. Thus, for the denoising, we used the erosion and dilatation method to achieve this task. The result is shown in Fig. 5(a). However, we still found that the outer edge was not smooth in the abdomen images. In order to solve this problem, we used the median filter which has the advantage of creating a smooth abdominal outer edge. The result is shown in Fig. 5(b). Finally, we used the abdominal fat area image as shown in Fig. 5(b) to find out the corresponding CT

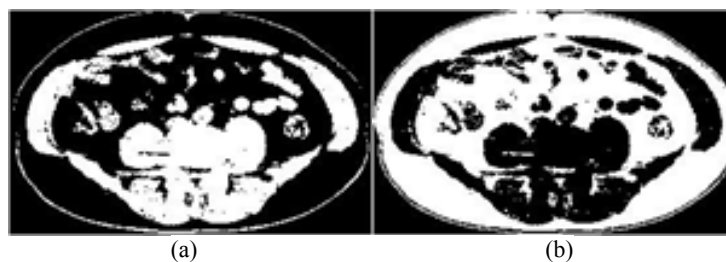value in the original image. The result is shown in Fig. 5(c).



(a)          (b)

**Fig. 4.** (a) Non-fat area image, and (b) is the resulting image obtained by XOR operator
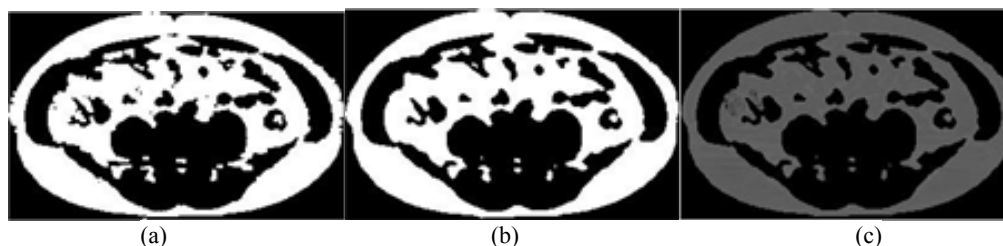


(a)        (b)        (c)

**Fig. 5.** (a) The result image after erosion and dilatation, (b) is the result image after Medium filter image and (c) is the TAT image before denoising

After performing the above mentioned methods, non-fat regions were measured. For removing non-fat regions, we again performed the image binarization on the TAT image as shown in Fig. 5(c). The threshold value which we used was the same as used at the binarized abdominal image as shown in Fig. 5(b). Thus we got a non-fat regions image as shown in Fig. 6(a). At last, we used the non-fat regions image to remove the non-fat regions within the TAT image. The result is shown in Fig. 6(b).



(a)          (b)
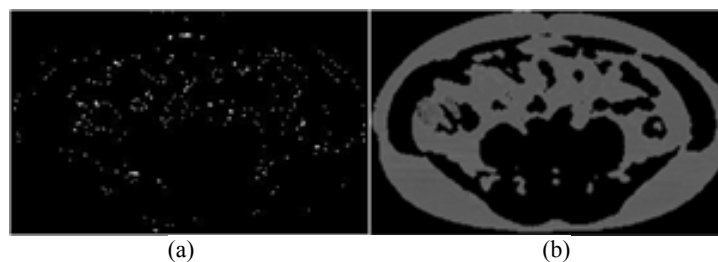
**Fig. 6.** (a) Non-fat regions image (b) TAT image

### B. SAT / VAT Area Extraction

In order to separate the SAT and VAT area from the TAT area, we had to find the boundary line between the SAT and VAT areas. Therefore, we performed edge detection on the binarized CT image as shown in Fig. 3(b). The result is shown in Fig. 7(a). Next, we used a connected component method to get the maximum connected component as shown in Fig. 7(b). The purpose of the above steps is to define the abdomen outer edge. After defining the abdominal outer edge, we performed edge detection on the TAT image to define all edges in the TAT area as shown in Fig. 7(c).



(a)        (b)        (c)
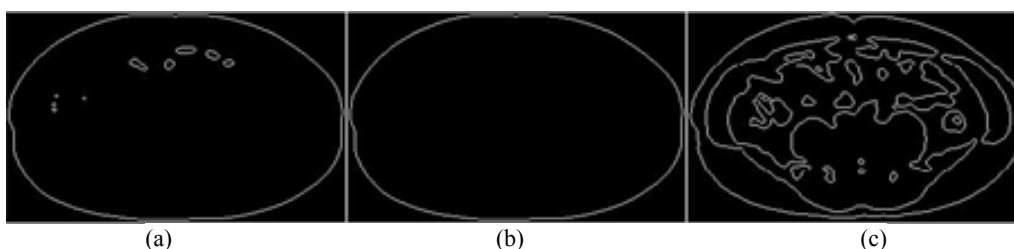
**Fig. 7.** (a) is abdomen edge, (b) is abdomen outer edge, and (c) is TAT edge image

Finally, we searched for the boundary line between SAT and VAT by applying the boundary line-seeking method. The boundary line-seeking process is shown in Fig. 8.
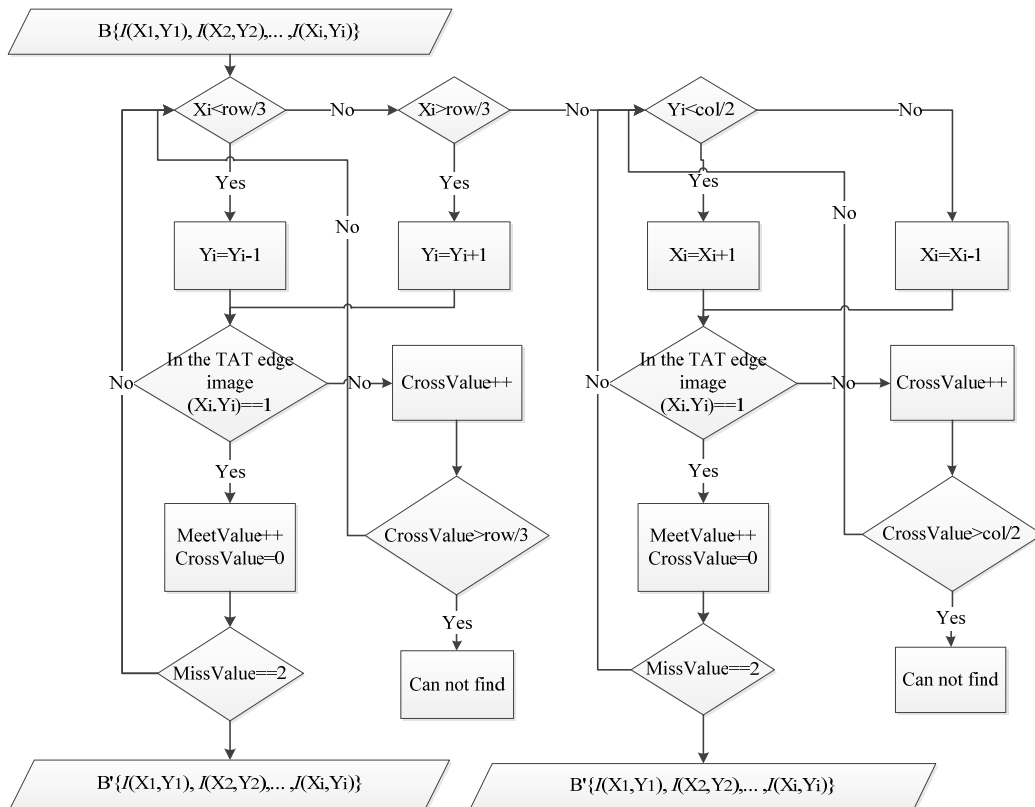
**Fig. 8.** The flowchart of boundary line-seeking.

In the boundary line-seeking method as shown in Fig. 8, the input B$\{$I($X_1$, $Y_1$), I($X_2$, $Y_2$), …, I($X_i$, $Y_i$)$\}$ indicates every dot of the abdominal outer edge, row indicates the length of the row of the TAT edge image and column indicates the length of the line of the TAT edge image. MeetValue indicates the number of times white points are touched, with initial value being zero and CrossValue indicates the distance between one white point and another, with initial value being zero.

At the beginning the system will first read every dot on the abdominal outer edge which is divided into six parts as showed in the location map in Fig. 9(a). Then based on the TAT edge image, we searched for the boundary line between SAT and VAT inwardly from the six parts mentioned above, as the chart in Fig. 9 (b) shows. When $X_i$ is smaller than row/3, we need to go downward to find the dot. When $X_i$ is greater than row×2/3, we need to go upward to find the dot. When $Y_i$ is smaller than column/2, we need to go right to find the dot.   When $Y_i$ is greater than column/2, we need to go left to find the dot. Next, we will decide after we move, whether the dot where we are on is white. If it is not white, CrossValue will increase by one. Then we will decide whether CrossValue is greater than the threshold values row/3 and column/2 set by us. If it is, our system will decide the boundary line has not been found; otherwise, it will keep searching. If the dot we are on after moving is white, MeetValue will increase by one, and meanwhile, CrossValue will set the initial value as zero. Then we will decide whether MeetValue is two. If it is, the system will decide one of the dots on the dividing line has been found; otherwise, it will keep searching until it finds it. During the process, we repeatedly search for the boundary line through this algorithm and eventually, will get an image of the boundary line as shown in Fig. 10(a).



(a)                                        (b)
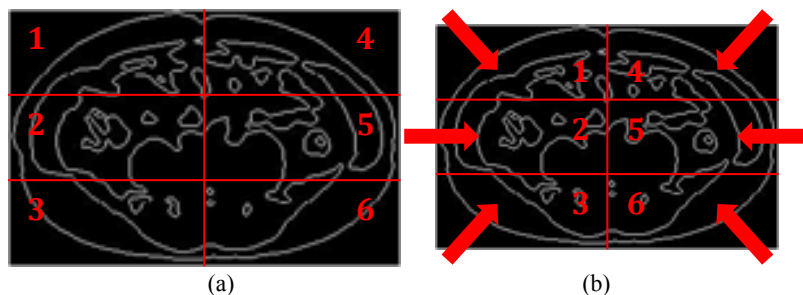
**Fig. 9.** (a) The six position of abdomen outer edge for seeking boundary line. (b) The direction map for boundary line-seeking.

Next, we have defined a preliminary boundary as shown in Fig. 10(a). But, we still could clearly discover within this image that the boundary is incomplete, and there is a lot of noise. It is not the real boundary. In order to remove the points which are not boundary between SAT and VAT area, we performed denoising two times using a $7\times7$ mask which centered around every point. Herein, this mask will perform a convolution action with the preliminary boundary image as shown in Fig. 10(a). It judges the pixel number within the boundary image in the window. When the pixel number in any direction of the eight direction from the center pixel is less than seven, the region will be regarded as the noise region. Therefore, the pixel value of all pixels within this region will be set as zero. Otherwise, it will be identified as a region without noise. Fig. 11 (a) shows the without-noise region and (b) shows the noise region. Fig. 10 (b) shows the result after performing noise region.



(a)                                        (b)

**Fig. 10.** (a) Preliminary boundary (b) Boundary after denoising



(a)                                        (b)
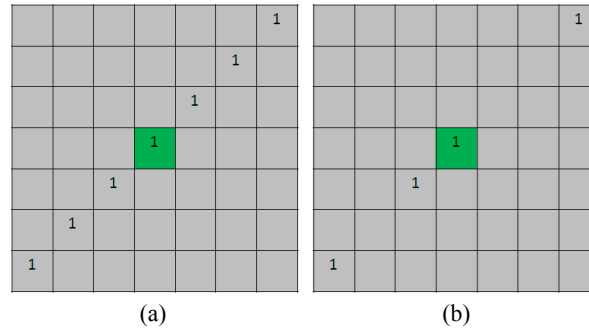
**Fig. 11.** (a) Without noise region (b) Noise region.

Next, we searched these points which we have to link in the boundary. In order to link these points, we developed a link algorithm for linking every two points. In this paper, the algorithm we proposed is shown Fig. 12.

*Linking Algorithm*

$Input : \{ P_0(X_0, Y_0), P'(X', Y') \}$

$Output : P_1(X_1, Y_1), P_2(X_2, Y_2), P_3(X_3, Y_3), \dots P_n(X_n, Y_n)$

$While \quad D > \sqrt{2}$

$\quad If \quad Angle > 30°$

$\qquad X_n = X_{n-1} + 1 \leftarrow V_x \ is \ positive$

$\qquad X_n = X_{n-1} - 1 \leftarrow V_x \ is \ negative$

$\quad End \ If$

$\quad If \quad Angle < 60°$

$\qquad Y_n = Y_{n-1} + 1 \leftarrow V_y \ is \ positive$

$\qquad Y_n = Y_{n-1} - 1 \leftarrow V_y \ is \ negative$

$\quad End \ IF$

$End \quad while$

$D \ \leftarrow The \ distance \ of \ P_{n-1} and \ P'$

$D > \sqrt{2} \ means \ P_{n-1} and \ P' \ is \ not \ connected$

$Angle \ \leftarrow The \ angle \ between \ D \ and \ V_y$

$V_x = X' - X_{n-1}$

$V_y = Y' - Y_{n-1}$

**Fig. 12.** Linking Algorithm

Where $P_0$ and $P'$ which represent two points to link as shown in Fig. 10(b). Because a straight line was used to link two points, it is not smooth and does not fit in with the real situation. Thus, using our proposed linking algorithm, we are able to connect all points which we have to link between $P_0$ and $P'$, and the boundary after performing linking algorithm is smoother. In the process of linking the two points, we assume that there is a virtual lower-right-triangle. If the angle near the $P_0$ is less than 30, it means that the horizontal vector is much longer so that we have to horizontally link, as shown in Fig. 13(a). If the angle near the $P_0$ is higher than 60 degrees, it means that the vertical vector is much longer so that we have to vertically link, as shown in Fig. 13(b). But, if the angle near the $P_0$ is between 30 degrees and 60 degrees, it means that two vectors are about equal so that we have to obliquely link. The boundary after using a linking algorithm is shown in Fig. 14 (a).



(a)                                    (b)
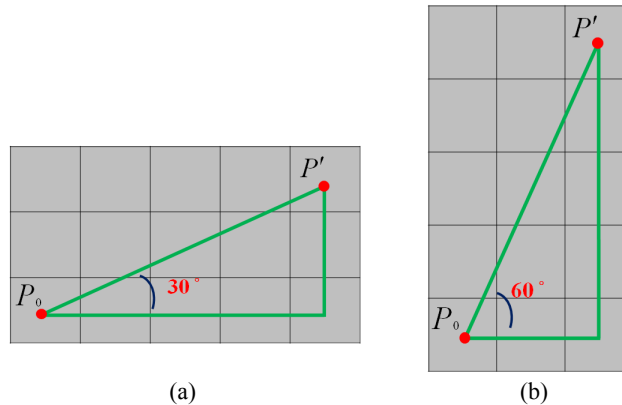
**Fig. 13.** (a) the angle near the $P_0$ is less than 30 (b) the angle near the $P_0$ is higher than 60 degrees

After getting the complete boundary line between the SAT and VAT area, we employed this boundary to define the SAT and VAT area from the TAT image as shown in Fig. 6(b). The result images are shown in Fig. 14(b) and (c), respectively.



(a)                                    (b)                                    (c)
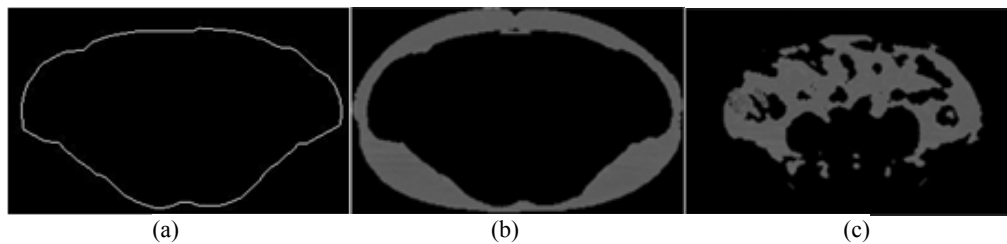
**Fig. 14.** (a) is the boundary line map after performing our proposed linking algorithm, (b) is SAT image, and (c) is VAT image

### 2.3    Calculation of Abdominal Fat

After getting the SAT and VAT image, our proposed system will start to calculate the quantity of abdominal fat. While the unit of the amount of abdominal fat obtained by our proposed is pixel, the real unit is not pixel. Hence, we will get the amount of abdominal fat per pixel from a radiologist. According to the result and all abdominal CT images per patient, the amount of abdominal fat will be calculated.

## 3 Results

The data format of images we used are $512 \times 512$ DICOM images obtained by low-resolution CT. Based on our proposed system, we can get three types of images: TAT, SAT, and VAT images. In our system, we used 200 images from 12 patients, including 10 to 20 slices for each patient, to test our proposed system. In the all of patient's image, the problem slices are filtered by professional radiologists. There are blurring problem in these filtered slices. The blurring problem is resulting from patient's breathing vibration. Next, in total processed image, Table 1 shows some results for explaining our proposed method. Conventionally, most physicians make their diagnosis of the CT slices by direct observation. Experienced radiologists may make a mismatch when drawing the contours between SAT and VAT. The segmentation accuracy of the extracted region by the proposed approach is evaluated by three criteria. The first criterion is three statistical evaluation indices of image

segmentation, including detection rate (DR), false alarm rate (FAR), and correction rate (CR) [18]. The second criterion is an empirical evaluation index evaluated by OCE [19]. The final criterion is artificial assessment evaluated by the two radiologists.

In the SAT and VAT images, we found that it will let the SAT area involve real VAT area if the boundary is not selected well. We know that this problem takes place in the fourth and seventh columns of Table 1. The reason why this problem happened is that the images we used are low-resolution CT images. Because of this reason, there is a lot of noise when we find the boundary line between SAT and VAT areas, resulting in taking the real boundary failure. We also cannot artificially change the image resolution. The only solution what we can do is to additionally create a new idea to improve the problems. But it does not mean that we do not have good results. The results excluding the fourth and seventh images of Table 1 are very good, and there are almost no gaps. Through analysis and comparison between the good and bad results, the noise interference is still a still problem we have to solve. Whether the results are good or bad we all must solve the problem and let our system performs much better.

The detection rate:
$$DR = \frac{TP}{TP + FN} \qquad (8)$$

The false alarm rate:
$$FAR = \frac{FP}{TN + FP} \qquad (9)$$

The correction rate:
$$CR = \frac{TP + TN}{TP + TN + FP + FN} \qquad (10)$$

In Table 2, we randomly choose ten SAT and VAT images from all the images of the abdomen and then do comparison between ground truth image, obtained by radiologist doctor to circumscribe correct region, and the image obtained by our proposed method. DR, FAR and CR in Table 3 are the average results calculated by us by using the Eq. (8) to (10), where DR represents the probability that the fat cut by our automation system is detected as fat cut manually, FAR represents the probability that non-fat cut automatically is classified as fat cut manually, and CR represents the probability that the fat images are classified correctly as a whole. There are several terms that are commonly used along with the description of DR, FAR and CR. They are true positive (TP), true negative (TN), false negative (FN), and false positive (FP). Here we also apply OCE (objective level consistency error), a method for detecting errors, to check the comparison of our proposed system and ground truth image. The result of OCE in Table 3 is calculated by using the equation (11) to (14). OCE is a new method for measuring errors and is aimed at detecting the object level of a segmented image and the ground truth image by quantifying the similarity. Therefore, we hope to do error tests by applying objective judgment of OCE to increase the usability of our proposed system. The OCE equations are as follows.

$$E_{g,s}(I_g, I_s) = \sum_{j=1}^{M} \left[ 1 - \sum_{i=1}^{M} \frac{|A_j \cap B_i|}{|A_j \cup B_i|} \times W_{ji} \right] W_j \qquad (11)$$

$$W_{ji} = \frac{\bar{\delta}(|A_j \cap B_i|)|B_i|}{\sum_{k=1}^{N} \bar{\delta}(|A_j \cap B_k|)|B_k|} \qquad (12)$$

$$W_j = \frac{|A_j|}{\sum_{I=1}^{M}|A_I|} \qquad (13)$$

$$OCE(I_g, I_s) = \min(E_{g,s}, E_{s,g}) \qquad (14)$$

where $I_g = \{A_1, A_2, ..., A_M\}$ represents a reference (manual) image and $A_j$ is the $j$th fragment in $I_g$. $I_s = \{B_1, B_2, ..., B_N\}$ represents the segmented image and $B_i$ is the $i$th fragment in $I_s$. Finally, $\delta(x)$ is the delta function whose value equals 1 if the input is 0 and whose value is 0 otherwise. $\bar{\delta}(x) = 1 - \delta(x)$.

For artificial assessment evaluation, we adopted and modified the grading rule method described from Kobashi [24]. The segmentation result of each image is graded as A, B, or C by comparing the match/mismatch from two radiologists. The grade "A" means the our proposed system is comparable to the visual observation, and the number of the mismatch is less than 15 pixels with no inclusion of a part of another organ, the grade "B" denotes that the result is acceptable, which is worse than A, but at least 70% of the abdominal fat in SAT or VAT is detected, and the grade "C" denotes that the detected abdominal fat in SAT or VAT region is less than 70%. This system was tested on 200 images from 10 patients. The examination results are shown in Table 4.

**Table 1.** Left column is TAT results images, middle column is SAT results images, and right column is VAT results images
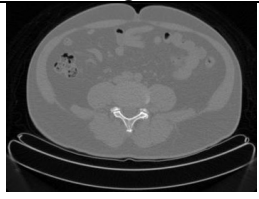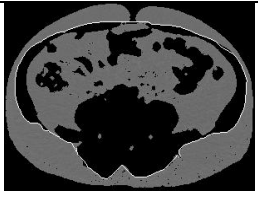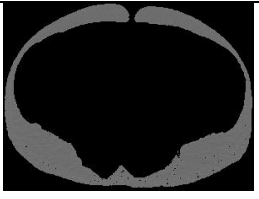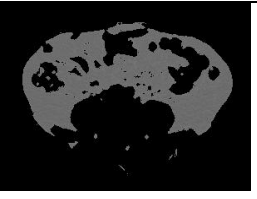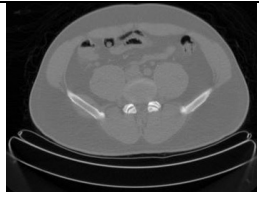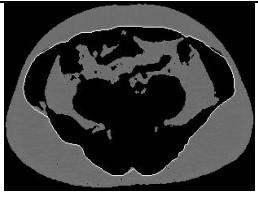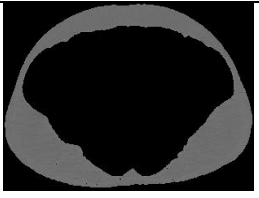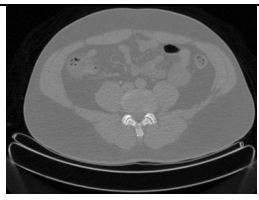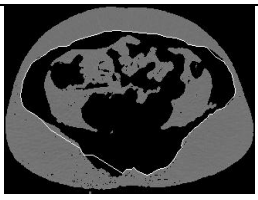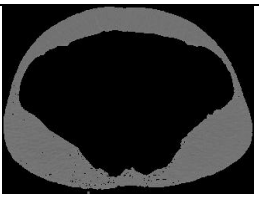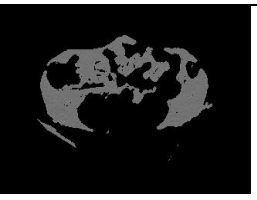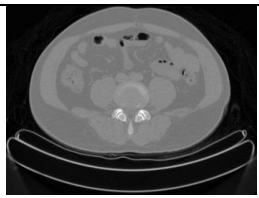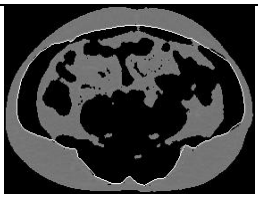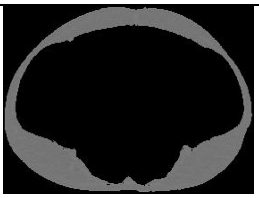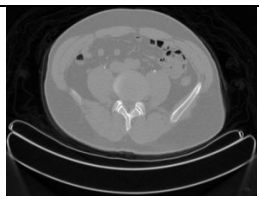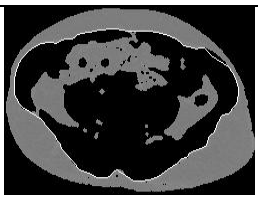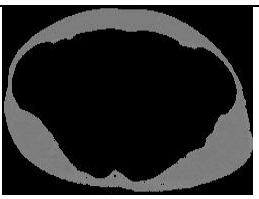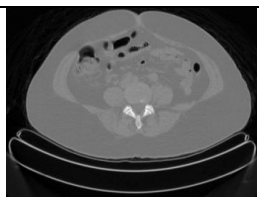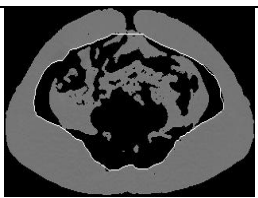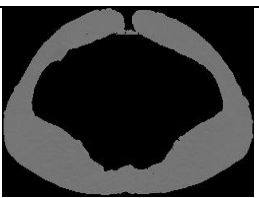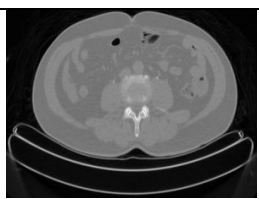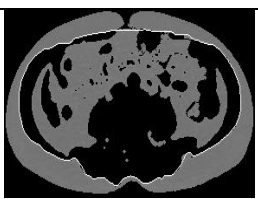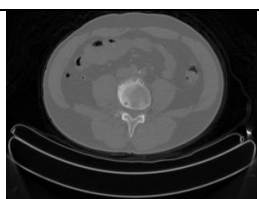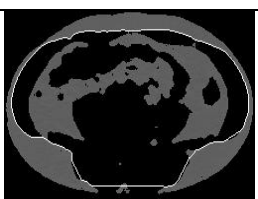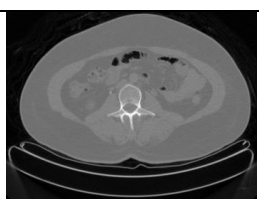
| Original | TAT | SAT | VAT |
|---|---|---|---|
|  |  |  |  |
|  |  |  |  |
|  |  |  |  |
|  |  |  |  |
|  |  |  |  |
|  |  |  |  |
|  |  |  |  |
|  |  |  |  |
|  |  |  |  |
| Original | TAT | SAT | VAT |

**Table 2.** Comparison between ground truth and our proposed system SAT and VAT

| Case | Ground truth( SAT) | Our proposed method (SAT) | The pixel number of difference | Ground truth (VAT) | Our proposed method (VAT) | The pixel number of difference |
|---|---|---|---|---|---|---|
| 1 | 28255 | 27964 | 291 | 7332 | 7343 | -11 |
| 2 | 27835 | 25944 | 1891 | 8296 | 7924 | 372 |
| 3 | 17659 | 15343 | 2352 | 17287 | 16933 | 354 |
| 4 | 17758 | 17183 | 575 | 8247 | 7737 | 510 |
| 5 | 19768 | 17953 | 1815 | 7811 | 7300 | 511 |
| 6 | 20245 | 19073 | 1172 | 8742 | 8313 | 429 |
| 7 | 24427 | 22871 | 1556 | 10717 | 10144 | 573 |
| 8 | 21289 | 20298 | 991 | 6786 | 6081 | 705 |
| 9 | 23603 | 23053 | 550 | 10310 | 8246 | 2064 |
| 10 | 16760 | 16519 | 241 | 13083 | 11808 | 1275 |

**Table 3.** The results of calculating DR, FAR, DR and OCE between ground truth image and the result image obtained by our

proposed method using the image of TAT, SAT and VAT.

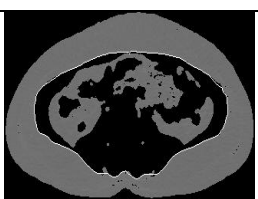| | DR | FAR | CR | OCE |
|---|---|---|---|---|
| TAT | 92.5% | 3.4% | 94.2% | 0.22 |
| SAT | 93.5% | 21.7% | 92.8% | 0.07 |
| VAT | 87.7% | 2.8% | 93.8% | 0.32 |

**Table 4.** Qualitative evaluation for 10 patients.

| Grade | SAT | VAT | TAT |
|---|---|---|---|
| A | 82% | 83% | 82.5% |
| B | 15% | 12% | 13.4% |
| C | 3% | 5% | 4.1% |

## 4 Discussions

Based on the statistics shown in Table 2, we discovered that the number of pixels segmented by our proposed system is very similar to the results from the pixels in the ground truth image segmented by radiologists. Furthermore, the results from the DR, CR and OCE in Table 3 have also shown that our proposed system is capable of successfully segmenting abdominal adipose images that matches the ground truth image. However, the SAT results in FAR have been disappointing, with the reason being that SAT is primarily composed of adipose tissue, with small quantities of non-fat tissues. This has easily caused the minority of non-fat components to be misclassified as adipose during our FAR analysis in SAT, which means that a small denominator and large numerator have led to the low detection rate. The closer the OCE component is towards the value of 0, the better the detection results, which also implies that our proposed method is similar to the image from the ground truth image, with SAT being the representative. But, the results from TAT and VAT are shown to be poorer than that in SAT, with the reason being that the segmentation in VAT is easily affected by the internal tissues and organs, result in our system to be unable to achieve complete segmentation. The variation in results is also due to the fact that OCE conducts overall detection based on "shape", whereas our detection is based on pixel value, thus there will be an error. From the results in Table 2 and Table 3, we can understand that the detection rate in CR has an average successful rate of above 92%, whereas the detection rate in OCE has an average success rate of above 80%.

From the results shown by the image as shown in Table 1, we discovered that if the boundary line with TAT is not selected correctly, the area that is originally of external adipose would be encompassed within the area of internal adipose. We can see clearly from the image results after the segmentation that there is an area removed in the image of the external adipose, while there is an additional area in the VAT image (which is not originally there). The errors have occurred as, when we search for the dividing line from the outside to the inside using edge line imagery, there will be some parts of the images revealing noise that are even beyond the boundary line,

causing a gap to appear in the middle of the edge, thus resulting in the failure to detect the correct edge during the detection process. This also implies that the image shown by the boundary line, after the gap has been filled, does not reflect the real area results. The most fundamental cause is that we have used low-resolution CT images in our research, thus these areas will face interference from the noise, and we were unable to use artificial means to resolve the resolution problem in the equipment.

However, this does not mean that our proposed method, under such conditions, is unable to produce excellent results. For instance, perfect segmentation has been achieved for the boundary lines in certain images as shown in Table 1, while there is almost no gap in the boundary lines and these lines also stick very closely to the contours of the interior area of external adipose. This allows the areas of internal adipose and external adipose to appear completely, while there is neither noise point nor interference in the final image results. After an analytical comparison between the good and poor image results, elimination of the noise interference problem due to low resolution is a goal that we have to achieve in the future. This paper has also utilized OCE in the conduct of error detection. It allows us to understand the correctness of our proposed system from another perspective.

## 5 Conclusions

This paper proposes an automatic segmentation system for measurement of abdominal fat. The input image of this system is obtained by a low resolution CT device. It can distinguish the SAT and VAT area from an abdominal image. There are two main algorithms in this paper. One is a boundary line-seeking algorithm. The other is a linking algorithm. We applied the proposed approach to 200 images from 10 patients with pathologies and evaluated the system performance qualitatively and quantitatively. The implementation time of our proposed system is within one second. And, its segmentation success rate is higher than 92% between automatic and manual segmentation on the 200 images considered. However, more work is necessary to validate the technique on a larger and more varied dataset.

## References

[1]    O.M. Abdulrahman, "Overweight and Obesity in Eastern Mediterranean Region: Prevalence and Possible Causes," *Journal of Obesity*, Vol. 2011, pp. 1-17, 2011.

[2]    R.M. Leech**,** S.A. McNaughton, A. Timperio, "The Clustering of Diet, Physical Activity and Sedentary Behavior in Children and Adolescents: A Review," *International Journal of Behavioral Nutrition and Physical Activity*, Vol. 11, pp. 4, 2014.

[3]    T. Lobstein, J.L. Rachel, "Child Overweight and Obesity in the USA: Prevalence Rates According to IOTF Definitions," *International Journal of Pediatric Obesity*, Vol. 2, pp. 62-64, 2007.

[4]    S.M. Lluis, A.B. Javier, P.R. Carmen, R.B. Lourdes, D.R. Alfonso, "Prevalence and Deteminants of Obesity in Spanish Children and Young People," *British Journal of Nutrition*, Vol. 96, pp.67-72, 2006.

[5]    A.M. Newman, "Obesity in Older Adults," *American Nurses Association*, Vol. 14, pp. 1, 2009.

[6]    C.L. Ogden, M.D. Carroll, L.R. Curtin, M.A. McDowell, C.J. Tabak, K.M. Flegal, "Prevalence of Overweight and Obesity in the United States," *The Journal of the American Medical Association*, Vol. 295, pp. 1549-1555, 2006.

[7]    K.M. Flegal, M.D. Carroll, C.L. Ogden, L.R. Curtin, "Prevalence and Trends in Obesity among US Adults," *The Journal of the American Medical Association*, Vol. 303, pp. 235-241, 2010.

[8]    L.C. Thomas, "Overweight and obesity in childhood – A special challenge for public health," *International Journal of Hygiene and Environmental Health*, Vol. 210, pp. 585-589, 2007.

[9]    X.J. Li, J.F. Youngren, B. Hyun, G.K. Sakkas, "Technical Evaluation of in Vivo Abdominal Fat and IMCL Quantification using MRI and MRSI at 3T," *Magnetic Resonance Imaging*, Vol. 26, pp. 188-197, 2008.

[10] A. Pednekar, A.N. Bandekar, I.A. Kakadiaris, "Automatic Segmentation of Abdominal Fat from CT Data," in *Proceedings of IEEE Workshops on Application of Computer*, Vol. 1, pp. 308-315, 2005.

[11] H. Chung, D. Cobzas, J. Lieffers, "Automated segmentation of muscle and adipose tissue on CT images for human body composition analysis," in *Proceedings of SPIE Medical Imaging: Visualization, Image-Guided Procedures, and Modeling*, Vol. 7261, pp. 197-205, 2009.

[12] Y. Jin, C. Imielinska, A.F. Laine, J. Udupa, W. Shen, S.B. Heymsfield, "Segmentation and evaluation of adipose tissue from whole body MRI scans," in *Proceedings of MICCAI 2013*, Vol. 2878 of LNCS,  pp. 635-642, 2003.

[13] H. Bertram, G. Thörmer, F. Dazinger, M. Raschpichler, N. Garnov, T. Kahn, "Software for fully automatic quantification of abdominal fat with manual correction option," *International Society for Magnetic Resonance in Medicine*, Vol. 19, pp. 848, 2011.

[14] A. Zhou, Y. Ding, R.W. McColl, P.T. Weatherall, Q. Peng, "Fully-Automated Abdominal Fat Quantification on Water-Saturated MRI," *International Society for Magnetic Resonance in Medicine*, Vol. 16, pp. 1518, 2008.

[15] A.S. Anderson, S. Caswell, "Obesity management — An opportunity for cancer prevention," *The Surgeon*, Vol. **7**, pp. 282-285, 2009.

[16] J.P. D'Auria, "Weighing In: Prevention of Childhood Overweight and Obesity," *Journal of Pediatric Health Care*, Vol. 25, pp. 26-30, 2011.

[17] S. Rayalam, J.Y. Yang, M.A. Della-Fera, C.A. Baile, "Novel Molecular Targets for Prevention of Obesity and Osteoporosis," *The Journal of Nutritional Biochemistry*, Vol. 22, pp. 1099-1104, 2011.

[18] Y.J. Zhang, "A Survey on Evaluation Methods for Image Segmentation," *Pattern Recognition*, Vol. 29, pp. 1335-1346, 1996.

[19] M. Polak, H. Zhang, M. Pi, "An Evaluation Metric for Image Segmentation of Multiple Objects," *Image and Vision Computing*, Vol. 27, pp. 1223-1227, 2009.

[20] H.H. Tsai, C.L. Chin, Y.C. Cheng , "Intelligent Pulmonary Embolism Detection System," in *Proceedings of International Conference on Biomedical Engineering and Informatics*, Vol. 24, pp. 471, 2012.

[21] S.Y. Wu, C.L. Chin, Y.S. Cho, Y.C. Chang, L.P. Hsu, "Intelligent Breast Tumor Detection System with Texture and Contrast features," *International Conference on Biomedical Engineering and Informatics*, Vol. 25, pp. 135, 2012.

[22] C.-T. Lin and C.-L. Chin, "Using Fuzzy Inference and Cubic Curve to Detect and Compensate Backlight Image, " *International Journal of Fuzzy Systems*, Vol. 8, No. 1, March 2006

[23] N. Otsu, "A Threshold Selection Method from Gray-Level Histograms," *IEEE Transactions on Systems, Man and Cybernetics*, Vol. 9, pp. 62-66, 1979.

[24] M. Kobashi , L.G. Shapiro, "Knowledge-based Organ Identification from CT images," *Pattern Recognition*, Vol. 28, pp. 475–491, 1995.